

Microlensing Maps for the Milky Way Galaxy

N. W. Evans and V. Belokurov

Theoretical Physics, Department of Physics, 1 Keble Road, Oxford, OX1 3NP, UK

ABSTRACT

At any instant, there are ~ 1000 microlensing events to sources brighter than 20th magnitude in the Milky Way Galaxy. Large-scale maps of the microlensing optical depth and the mean timescale are constructed for a number of models of the Galactic bar and disk, incorporating the effects of streaming and spiral structure. Freudenreich's model can reproduce the high optical depths towards the Bulge. It is also in good agreement with the data towards the spiral arms (except for the field γ Norma). Spiral structure tends to increase the optical depth by $\lesssim 20\%$ and the mean timescale by $\lesssim 100\%$. Different bar morphologies give characteristically different shaped contours, especially at low Galactic latitudes ($|b| < 2^\circ$). These could be traced out with a K band microlensing survey, consuming ~ 100 minutes per night on a telescope like VISTA.

Subject headings: Galaxy: structure – Galaxy: kinematics and dynamics – gravitational lensing

1. INTRODUCTION

Microlensing surveys of the Galaxy are important because they delineate the mass distribution directly. The total number of events identified by the OGLE and MACHO collaborations towards the Galactic Bulge now exceeds a thousand (e.g., Wozniak et al. 2001; Alcock et al. 2000). The identification of events towards spiral arms has been reported by the EROS and OGLE collaborations (Mao 1999; Derue et al. 2001). Maps of optical depth as a function of Galactic latitude and longitude were first drawn by Evans (1994). Subsequently, a number of authors emphasised the importance of exploiting information on the spatial variation of the optical depth (e.g., Han & Gould 1995; Zhao, Spergel & Rich 1996; Gyuk 1999).

Microlensing searches are being done, or will be done in the near future, in almost any longitude direction. The first of the next generation experiments is the OGLE III venture (see “<http://sirius.astro.uw.edu.pl/ogle/>”) which uses an 8k MOSAIC camera with a field

of view equal to $35' \times 35'$. The future holds still greater promise with the advent of the new class of survey telescopes like the VST (“<http://www.eso.org/projects/vst/>”) and VISTA (“<http://www.vista.ac.uk>”). VISTA has a field of view of 2.25 square degrees in the optical, while the VST has a smaller, but still substantial, field of view of 1 square degree. So, there is a need for large-scale maps of both the microlensing optical depth and the mean timescale for the Galaxy. These maps can be used to pick target fields, to plan search methodologies for future experiments and to assess what can be learnt about the structure of the Milky Way from the distribution of microlensing events.

2. MAPS OF THE GALAXY

We study three models of the inner Galaxy. The starting point of all three models is the same, namely the infrared surface brightness maps seen by the DIRBE instrument on the COBE satellite. The first is the model of Binney, Gerhard & Spergel (1997), which is partially revised in Bissantz et al. (1997). Here, the observed luminosity at ~ 240 microns, which is dominated by thermal emission from dust, is used to deduce the three-dimensional spatial distribution of the dust. This gives a short, flattened, cuspy bar with axis ratio $1 : 0.3 : 0.3$ and with a viewing angle $\phi_0 = 20^\circ$. The second is the model of Freudenreich (1998). Here, a mask of areas believed to be contaminated with dust is constructed from maps of color variations. The mask is used to excise portions of the DIRBE data and the remainder of the data is fitted. Note that the mask removes almost all of the data within $|b| \lesssim 5^\circ$ for longitudes within 90° of the Galactic Center (see Figure 1 of Freudenreich’s paper). This gives an extended, diffuse, swollen bar with axis ratio $1 : 0.37 : 0.27$ and with a viewing angle $\phi_0 = 14^\circ$. The disk has a central hole with a radius of ~ 3 kpc. The third is the E2 model of Dwek et al. (1995), as partially revised by Stanek et al. (1997). The density contours are stratified on concentric ellipses with axis ratio $1 : 0.42 : 0.28$ with a viewing angle $\phi_0 = 24^\circ$. In correcting for dust, Dwek et al. assumed a uniform foreground screen. The bar is less massive and less elongated than Freudenreich’s and the disk does not have a central hole. To ensure a fair comparison, all three models are normalized to have the same total mass of $1.5 \times 10^{10} M_\odot$ within 2.5 kpc. Optical depths scale in rough proportion with total mass, and so our results can be easily converted to other preferred values. The three models are illustrated in Figure 1. Cuts through the principal plane of the bar and along the line of sight to the Galactic Center are shown. Table 1 shows the masses of the components in the three models. Freudenreich’s bar is the most massive, Binney et al.’s the least massive.

EROS and OGLE are looking towards spiral arms. Accordingly, we include the effects

of spiral arms in our calculations. We assume that the inner spiral pattern is two-armed and given by multiplying the density by eqn (2) of Binney et al. (1997), namely

$$1 + \epsilon \cos^6(\phi - 0.95(r - r_{\min}) - \phi_0), \quad \epsilon = \tanh(r - r_{\min}). \quad (1)$$

Here, r_{\min} is proportional to the length of the bar and is 1.5 kpc for Binney et al.’s bar, 2.25 kpc for Freudenreich’s and 1.7 kpc for Dwek et al.’s. This density factor is applied between r_{\min} and $r_{\max} = 3.5$ kpc. The outer spiral pattern is four-armed and given by $1 + 2\epsilon \cos^6(2\phi - 1.1(r - r_{\min}) - 15^\circ)$ between $r_{\min} = 4.1$ kpc and $r_{\max} = 8.5$ kpc. The phase and the wavenumber of the inner and outer spirals are chosen to match the longitudes of the principal spiral arms given by Englmaier (2000). The arm/interarm contrast is 2 for the inner and 3 for the outer spiral (cf. Rix & Rieke 1993). This is reasonable for a young population, but an overestimate for old low mass stars that may make up the bulk of the lensing population. Our results on the effects of spirality are upper limits.

Microlensing maps show contours of the source-averaged microlensing optical depth $\langle \tau \rangle$ computed via (Kiraga & Paczyński 1994)

$$\langle \tau \rangle = \frac{\int_0^\infty \rho(D_s) \tau(D_s) D_s^{2+2\beta} dD_s}{\int_0^\infty \rho(D_s) D_s^{2+2\beta} dD_s}, \quad (2)$$

where D_s is the source distance and ρ is the density of deflectors. For red clump stars, $\beta \approx 0$; for main sequence stars, $\beta \approx -1$. Red clumps stars are bright and distinctive residents of the bar (e.g., Paczyński & Stanek 1998). Figure 2 shows contours of optical depth to the red clump in the three models. The dotted contours show the effect of including the spiral structure. The amplification caused by spirality varies according to the line of sight but it is typically $\sim 20\%$. Of the three, Binney et al.’s gives the least symmetric microlensing map, especially close to the Galactic plane where the gradients are very steep. Freudenreich’s is the most symmetric, as it possesses the smallest viewing angle. The boxes mark the two locations where the optical depth of bar stars has been measured. The first is $\ell = 3.9^\circ, b = -3.8^\circ$ where Popowski et al. (2000) report $2.0 \pm 0.4 \times 10^{-6}$ for the optical depth to the red clump stars. The second is $\ell = 2.68^\circ, b = -3.35^\circ$ where Alcock et al. (2000) report $3.2 \pm 0.5 \times 10^{-6}$ for the optical depth to bar stars. The value of the optical depth at $\ell = 3.9^\circ, b = -3.8^\circ$ contributed by each component in the three models is recorded in Table 2. Freudenreich’s model is in good agreement with the two measurements of optical depth to the bar sources.

Even though all three models have the same total mass within 2.5 kpc, Freudenreich’s model has the higher optical depth because the bar is more extended. Notice that the shape of the contours in Figure 2 becomes very similar for all three models once $|b| > 4^\circ$. This makes it challenging to characterize the bar morphology on the basis of data from the observed fields. One qualm is that Freudenreich excised most of the DIRBE data within $|b| \lesssim 5^\circ$ of the

Galactic plane. In this region, his model is entirely extrapolated from the light distribution at higher latitudes and so may be unreliable. Binney et al.’s model reproduces the strong concentration in the light near the Galactic plane. It lies within $\approx 2\sigma$ of Popowski et al.’s measurement when spiral structure is included. Dwek et al.’s model with spiral structure is just outside 1σ . Can we modify Binney et al.’s model to reproduce the microlensing optical depth data? To get agreement with the data, the bar needs to be made both longer and fatter. For example, changing the axis ratio to $1 : 0.6 : 0.4$ (as originally envisaged in Binney et al. 1997) and increasing the total mass within 2.5 kpc by 50% gives a model in reasonably good agreement (namely $\tau = 1.5 \times 10^{-6}$ at $\ell = 3.9^\circ, b = -3.8^\circ$ excluding spiral structure; this rises to 1.8×10^{-6} when spiral structure is included).

Figure 3 shows the contours of optical depth to all sources in the inner Galaxy using Freudenreich’s bar. The Galactic disk has a sech-squared vertical profile with scaleheight 167 pc and an exponential horizontal profile with scalelength 2.5 kpc. The insets show the details of three areas towards the Scutum, Norma and Musca spiral arms that are being monitored by the EROS group. We see that there is a factor of ~ 6 variation in the optical depth across the EROS fields towards all three spiral arms. Freudenreich’s bar is so distended that it causes a thickening of the optical depth contours even at longitudes well away from the center. We can exploit the maps to estimate the number of ongoing microlensing events of stars brighter than 20th magnitude in the Milky Way. At any instant, there are ~ 1000 microlensing events, where we have allowed for extinction in the same manner as Belokurov & Evans (2002). Table 3 compares the predictions of the three models with the data provided by EROS. Notice that Freudenreich’s model is in excellent agreement with the data, except for the field γ Norma, where the optical depth is about 2σ away from the data.

3. TIMESCALE MAPS

It is also interesting to build maps of the mean Einstein crossing timescale. We assume that the mass function of the bar (or disk) is a power-law between $0.01 M_\odot$ and $0.5 M_\odot$ with index -1.33 (or -0.54) as suggested by Zoccali et al. (2001). Let (x, y, z) define coordinates along the major, intermediate and minor axis of the bar. We calculate the average velocity dispersions required to reproduce the shape of Freudenreich’s bar guided by the tensor virial theorem (e.g., Han & Gould 1995, Blum 1996). We assume that stars on the front side of the bar move along the major axis with a streaming velocity of $\langle v_x \rangle = 50 \text{ km s}^{-1}$, while stars on the back side move with $\langle v_x \rangle = -50 \text{ km s}^{-1}$ and we adjust the dispersion σ_x to preserve the total kinetic energy required by the virial theorem. With these assumptions, the velocity distribution is Gaussian about the streaming velocity with dispersions $\sigma_x =$

100 km s⁻¹, $\sigma_y = 80$ km s⁻¹, $\sigma_z = 68$ km s⁻¹. For the disk lenses, the random component has $\sigma_R = 34$ km s⁻¹, $\sigma_\phi = 21$ km s⁻¹, $\sigma_z = 18$ km s⁻¹ about a mean velocity $\langle v_\phi \rangle$ of 214 km s⁻¹ (see e.g., Edvardsson et al. 1993; Belokurov & Evans 2002). Although small velocity perturbations will be associated with the spiral arms, these are neglected in our calculations.

Figure 4 shows contours of the mean timescale for events with sources and lenses in either the disk or Freudenreich’s bar, including (dotted lines) and excluding (full lines) the spiral structure. The mean timescale is shortest towards the Galactic Center and becomes longer at increasing Galactic longitudes. This is easy to understand because the motion of the lens is directed more and more along the line of sight at larger longitudes and so the transverse velocity is typically smaller. Notice that spiral structure has a dramatic effect on the mean timescale. For example, at Baade’s Window, the mean timescale is increased by a factor of $\sim 100\%$ on incorporating the effects of spirality. Figure 5 shows the inner $20^\circ \times 20^\circ$ in Freudenreich’s model including (dotted lines) and excluding (full lines) the effects of bar streaming. This detail is drawn for sources in the bar only, and so the asymmetry in the map is substantial. Streaming is an important effect because it removes kinetic energy from random motions and places it in systematic motions that are directed almost along the line of sight. There is an increasing gradient in the mean timescale from the near-side to the far-side of the bar. This is a geometric effect, in that lines of sight to the near-side are more nearly perpendicular to the major axis than lines of sight to the far-side. Popowski et al. (2000) report that about 40 % of the optical depth is in events with timescales > 50 days and that this is at odds with standard Galactic models. By contrast, we find that long timescale events are to be expected when streaming is taken into account in the modelling.

4. CONCLUSIONS

We have drawn large scale maps of the optical depth and timescale distribution for microlensing in the Galaxy. Freudenreich’s bar does give a reasonable representation of the microlensing data to the Bulge. It recovers the optical depth towards the spiral arms (with the exception of γ Norma). However, Freudenreich’s model is hollow. Stars otherwise expected to be in the central parts of the disk can instead be used to augment the bar where they are efficient at microlensing.

As pointed out by Gould (1995), microlensing surveys in the K band would be very valuable to distinguish between models. This is all the more true given the capabilities of the new generation of survey telescopes. VISTA has a field of view of 0.5 square degrees in the K band. Assuming that the seeing is $0.8''$ in Chile and scaling the results of Gould

(1995), then we estimate that VISTA will monitor $\sim 1.5 \times 10^6$ stars in a single field of view for crowding-limited K band images towards the Bulge. This means that we are probing the luminosity function down to $K \sim 16$, assuming 3 magnitudes of extinction. Photometry accurate to 3% for a $K \sim 16$ star will take ~ 1 minute on VISTA. Hence, a K band survey of a $5^\circ \times 5^\circ$ field close to the Galactic Center will take ~ 100 minutes every night, allowing 50 minutes for readout, slew and guide star acquisition time. So, a K band microlensing survey of the inner Galaxy is an attractive and feasible proposition with VISTA.

NWE is supported by the Royal Society and VB acknowledges financial help from the Dulverton Fund. We thank Bohdan Paczyński and Shude Mao for emphasizing to us the importance of large-scale maps, as well as James Binney for discussions on the structure of the Galactic bar. The anonymous referee is thanked for a helpful report.

REFERENCES

- Alcock C. et al. 2000, ApJ, 541, 734
- Belokurov V., Evans N.W., 2002, MNRAS, in press (astro-ph/0112243)
- Binney J., Gerhard O., Spergel D. 1997, MNRAS, 288, 365
- Bissantz N., Englmaier P., Binney J., Gerhard O.E. 1997, MNRAS, 289, 651
- Blum R. 1995, ApJ, 444, L89
- Derue F. et al. 2001, AA, 373, 126
- Dwek E. et al. 1995, ApJ, 445, 716
- Edvardsson B., Andersen J., Gustafsson B., Lambert D.L., Nissen P.E., Tomkin J. 1993, A&AS, 102, 603
- Englmaier P., 2000, Rev Modern Astronomy, 13, 97
- Evans N.W., 1994, ApJ, 437, L31
- Gould A. 1995, ApJ, 446, L71
- Gyuk G. 1999, ApJ, 510, 205
- Han C., Gould A. 1995, ApJ, 449, 521

Kiraga M., Paczyński B. 1994, ApJ, 430, L101

Mao S. 1999, AA, 350, L19

Paczyński B., Stanek K.Z. 1998, ApJ, 494, L219

Popowski P., et al. 2000, In Menzies J.W., Sackett P.D. eds, Proc. Microlensing 2000, ASP Conference Series, in press (astro-ph/0005466)

Rix H.W., Rieke M.J. 1993, ApJ, 418, 123

Stanek K.Z., Udalski A., Szymanski M., Kaluzny J., Kubiak M., Mateo M., Krzeminski W. 1997, ApJ, 477, 163

Wozniak P.R., Udalski A., Szymanski M., Kubiak M., Pietrzynski G., Soszynski I., Zebrun K. 2001, Acta Astronomica, 51, 175

Zhao H.S., Rich R.M., Spergel D.N. 1996, MNRAS, 282, 175

Zoccali M., Cassisi S., Frogel J.A., Gould A., Ortolani S., Renzini A., Rich R.M., Stephens A.W. 2000, ApJ, 530, 418

| Model | bar < 2.5 kpc | disk < 2.5 kpc | bar+disk < 2.5 kpc | disk < 8.5 kpc | inner spiral 3.5 kpc | outer spiral 8.5 kpc |
|--------------|------------------|-------------------|-----------------------|-------------------|-------------------------|-------------------------|
| Binney et al | 0.5 | 1.0 | 1.5 | 3.2 | 0.3 | 0.9 |
| Freudenreich | 1.1 | 0.4 | 1.5 | 3.2 | 0.2 | 1.2 |
| Dwek et al | 0.9 | 0.6 | 1.5 | 2.6 | 0.2 | 0.9 |

Table 1: This table shows the mass (in units of $10^{10} M_{\odot}$) in different components of the Galaxy in the three models. The fifth column is the additional mass within 2.5 kpc caused by the inner spiral alone. The sixth column is the additional mass within 8.5 kpc caused by the outer spiral alone.

| source | bar | bar | bar | bar+disk | bar+disk | disk |
|--------------|-----|-----------|-----------|-----------|-----------|-----------|
| lens | bar | disk | bar+disk | bar+disk | disk | disk |
| Binney et al | 0.3 | 0.6 (0.9) | 0.9 (1.2) | 0.7 (0.8) | 0.5 (0.6) | 0.4 (0.5) |
| Freudenreich | 1.0 | 0.9 (1.4) | 2.0 (2.4) | 1.3 (1.6) | 0.7 (1.0) | 0.4 (0.5) |
| Dwek et al | 0.6 | 0.6 (0.9) | 1.2 (1.5) | 1.0 (1.1) | 0.5 (0.7) | 0.4 (0.6) |

Table 2: Optical depth towards $\ell = 3^\circ.9, b = -3^\circ.8$ in units of 10^{-6} . Recall that Popowski et al.’s (2000) value for the optical depth to the red clump is $2.0 \pm 0.4 \times 10^{-6}$, which should be compared to the numbers in the third column. The figures in parentheses include the effects of spiral structure. The extra enhancement in the optical depth comes mainly from the extra mass in the spiral models.

| Direction | θ Mus | γ Nor | γ Sct | β Sct |
|--------------|--------------|------------------------|------------------------|-------------|
| EROS | < 0.68 | $0.27^{+0.30}_{-0.17}$ | $1.64^{+0.92}_{-0.74}$ | < 1.03 |
| Binney et al | 0.32 (0.56) | 0.48 (0.69) | 0.79 (1.07) | 0.60 (0.83) |
| Freudenreich | 0.47 (0.71) | 0.78 (1.18) | 1.11 (1.43) | 0.95 (1.23) |
| Dwek et al | 0.34 (0.61) | 0.51 (0.72) | 0.85 (1.13) | 0.64 (0.90) |

Table 3: Optical depth towards spiral arms in units of 10^{-6} . The figures in parentheses include the effects of spiral structure. The numbers should be compared with the experimental data provided by the EROS collaboration (Derue et al. 2001) in the second line.

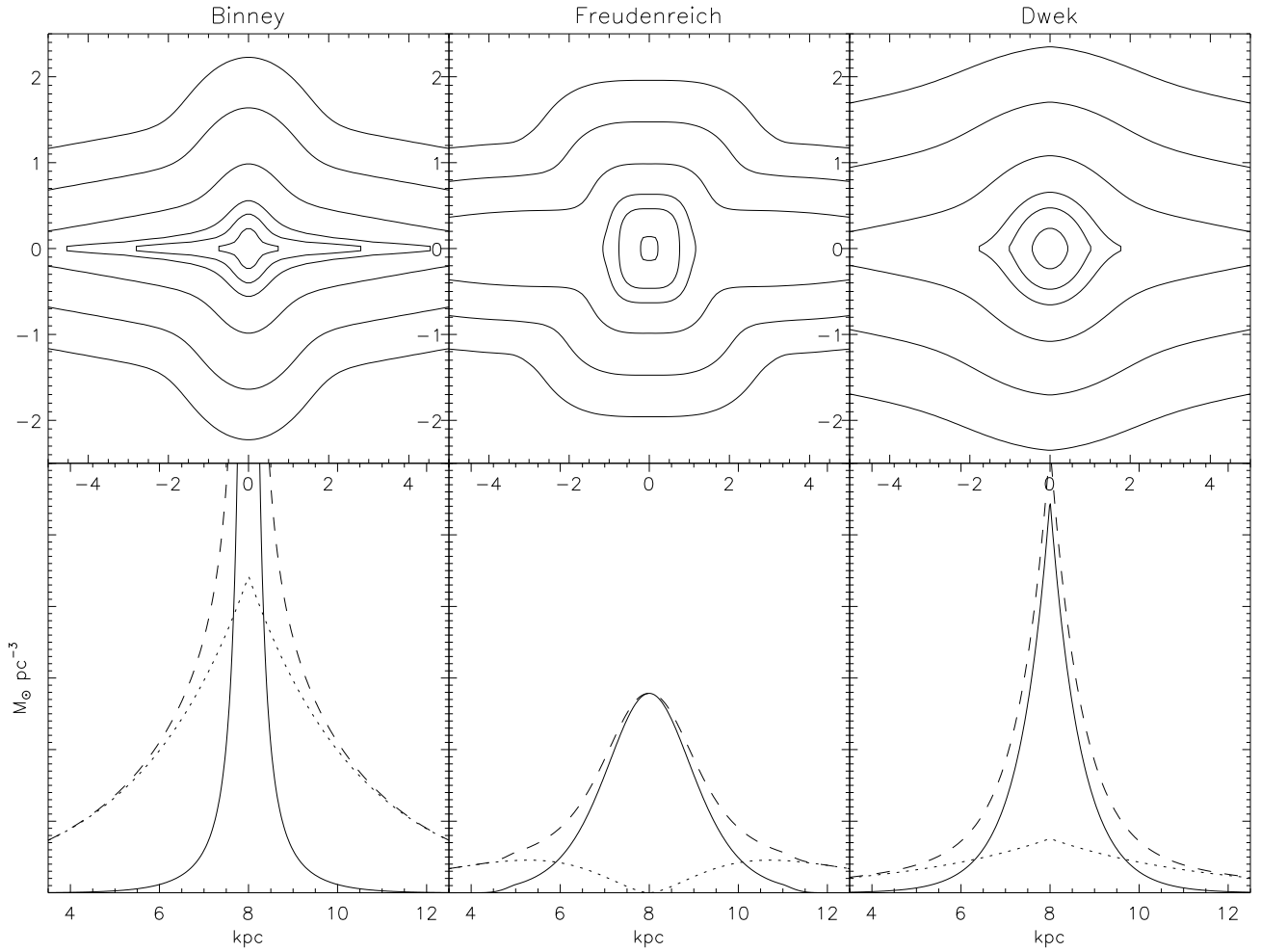


Fig. 1.— Upper panels show slices through the principal plane of the bars of Binney et al., Freudenreich and Dwek et al. The contour levels are $(10^{-3}, 10^{-2}, 10^{-1}, .5, 1, 2.5) M_{\odot} \text{pc}^{-3}$. Lower panels show the density contributions of the bar (full line), disk (dotted line) and total (dashed line) along the line of sight to the Galactic Center

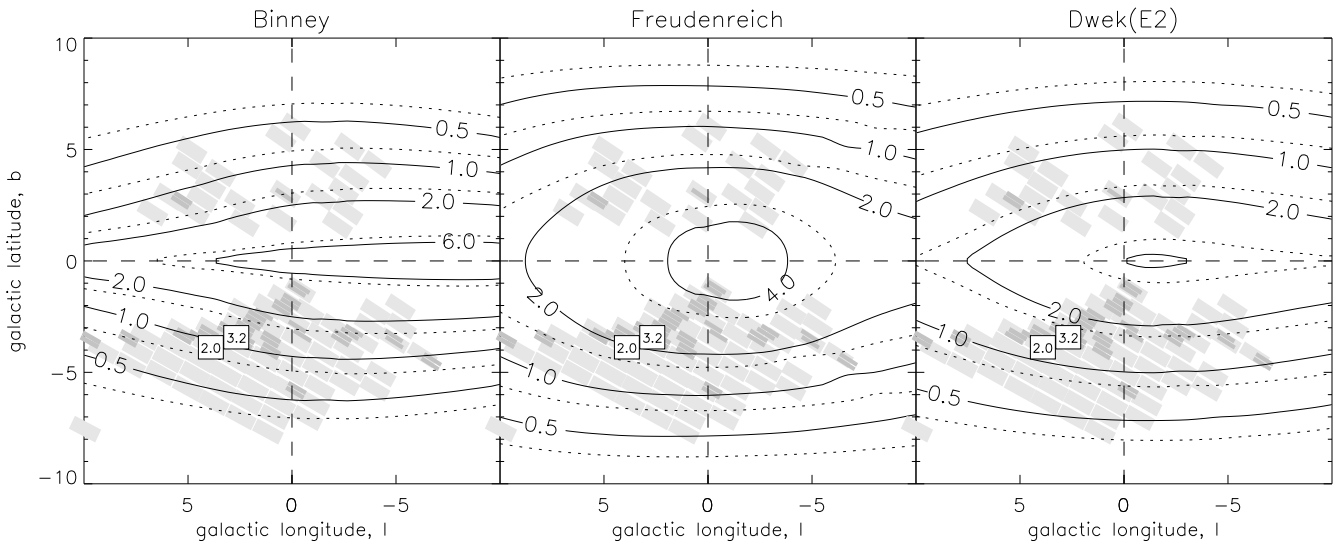


Fig. 2.— Contours of microlensing optical depth to the red clump giants (in units of 10^{-6}) in the three bar models, excluding (full lines) and including (dotted lines). The optical depths reported by Alcock et al. (2000) and Popowski et al. (2000) are shown in boxes. Light (dark) gray boxes correspond to EROS (OGLE II) fields.

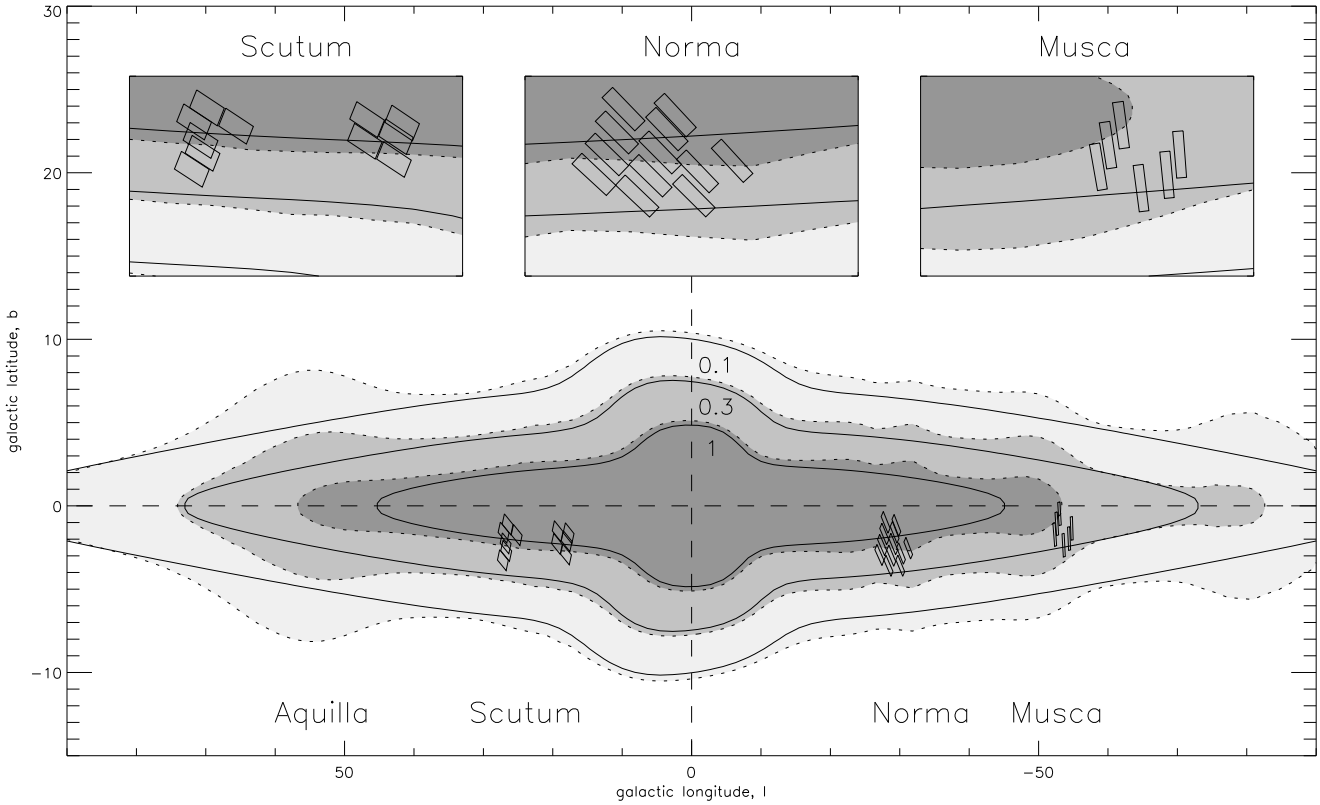


Fig. 3.— Contours of microlensing optical depth to all sources (in units of 10^{-6}) in Freudenreich’s model, excluding (full lines) and including (dotted lines) spiral structure. The insets show the details of EROS fields towards the Scutum, Norma and Musca spiral arms.

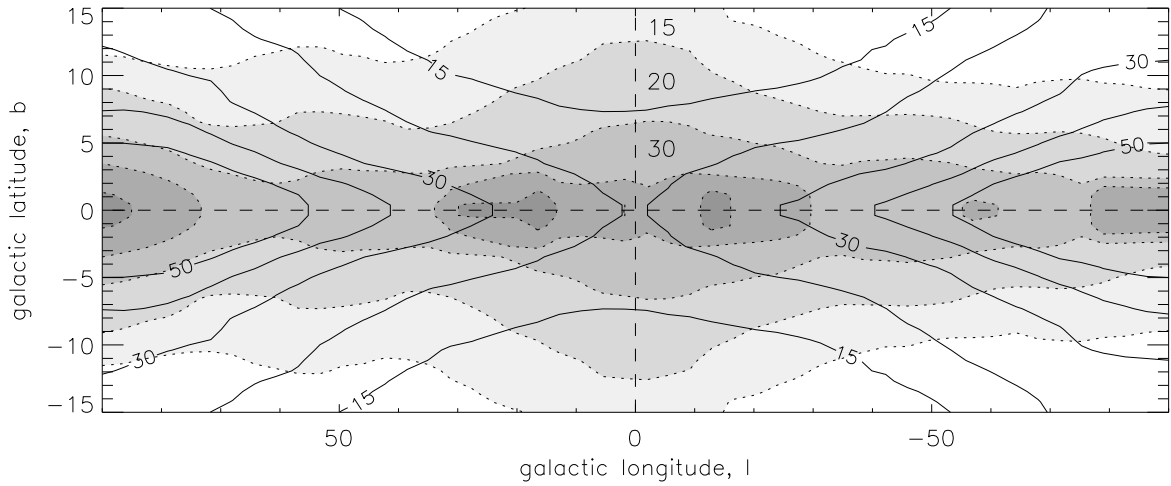


Fig. 4.— Contours of mean timescale (in days) for microlensing events with sources and lenses lying in either the disk or Freudenreich’s bar. The timescale is the time taken to cross the Einstein radius. The full lines exclude the contribution of spiral structure, the dotted lines include the contribution. The contour levels are at 15, 20, 30, 40 and 50 days.

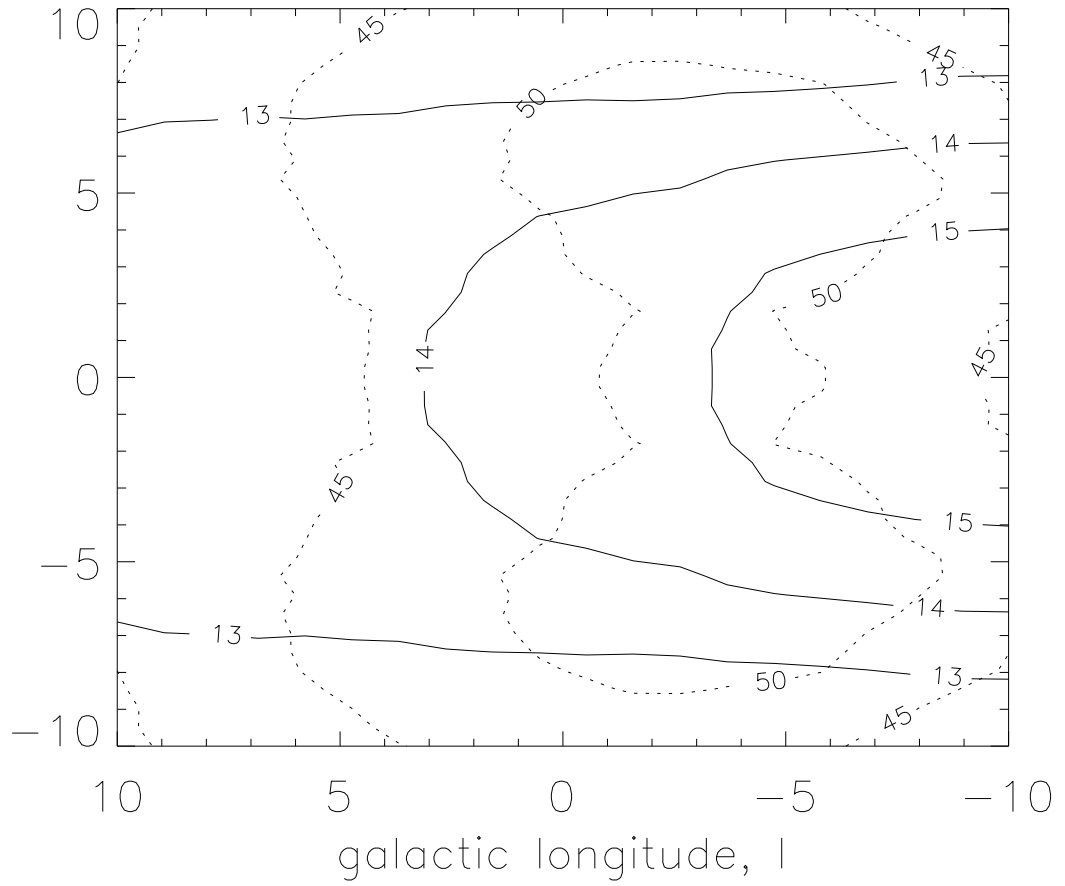


Fig. 5.— Contours of mean timescale (in days). The sources lie in the bar alone (Freudenreich’s model), the lenses may lie in either the disk or the bar. The full lines exclude the contribution of bar streaming, the dotted lines include the contribution.